Chinese Chemical Letters 33 (2022) 4101–4106

Contents lists available at ScienceDirect

Chinese Chemical Letters

journal homepage: www.elsevier.com/locate/cclet

Facile synthesis and *in vivo* bioimaging applications of porphyrin derivative-encapsulated polymer nanoparticles

Mengfei Hou[a,1], Wandi Chen[a,1], Junkai Zhao[a,b,1], Deshen Dai[a], Mo Yang[c], Changqing Yi[a,*]

[a] *Guangdong Provincial Engineering and Technology Center of Advanced and Portable Medical Devices, School of Biomedical Engineering, Sun Yat-sen University, Shenzhen 518107, China*

[b] *State Key Laboratory of Oncology in South China, Collaborative Innovation Center For Cancer Medicine, Sun Yat-sen University Cancer Center, Guangzhou 510060, China*

[c] *Department of Biomedical Engineering, The Hong Kong Polytechnic University, Hong Kong, China*

ARTICLE INFO

Article history:
Received 28 August 2021
Revised 16 January 2022
Accepted 17 January 2022
Available online 23 January 2022

Keywords:
Porphyrins
Fluorescence imaging
Photodynamic therapy
Theranostics

ABSTRACT

Fluorescence (FL) imaging guided photodynamic therapy (PDT) is becoming highly desirable for personalized therapy and precision medicine. In this study, fluorescent polymer nanoparticles TCPP@PEI/PGA were facilely synthesized through electrostatic interaction-mediated self-assembly of porphyrins tetra(4-carboxyphenyl)porphine (TCPP) and polyethylenimine (PEI), and subsequent surface modification with γ-poly(glutamic acid) (γ-PGA). TCPP served a dual function as the FL imaging probe and the photosensitizer. The as-prepared TCPP@PEI/PGA nanoparticles showed excellent water-solubility and biocompatibility, while having outstanding capabilities of *in vivo* bioimaging and $^1O_2$ generation. FL bioimaging of mice and effective killing of CT 26 cells as well as CT 26 tumor-bearing mice upon laser irradiation were successfully demonstrated when using TCPP@PEI/PGA as theranostic nanoprobes. This study provides a simple but robust method to design and synthesize porphyrin-based polymer nanoparticles for theranostics.

Due to its noninvasive, effective antitumor, and low adverse effects, photodynamic therapy (PDT) is becoming attractive in cancer treatment [1–5]. During PDT, photosensitizers (PS) are used to convert light into intracellular reactive oxygen species (ROS) to destroy tumor cells. However, the phototoxicity to normal tissues and high risk of tumor recurrence limits the clinical translation of PDT [6–8]. In order to address this critical issue, theranostic probes which can realize imaging-guided therapy are attracting more and more research attentions, due to the features of guidance of external lights to precisely irradiate tumor lesion sites and subsequent monitoring of treatment outcomes simultaneously [9,10]. Among various imaging methods, fluorescence imaging (FL) has shown great potential in the guidance of PDT as well as surgical operation, thanks to its capability of real-time *in vivo* imaging with subcellular resolution and single cell sensitivity [11–13]. Therefore, effective PS agents which integrate the capabilities of FL imaging and photo-induced ROS generation are highly desirable for personalized therapy and precision medicine.

Nowadays, porphyrins [14–16], BODIPY [17,18], Cyanine compound [19,20], are extensively used as effective PS agents for FL imaging-guided PDT. Especially, porphyrin derivatives are extensively used for FL imaging as well as PDT, owing to their excellent characteristics such as high vascular permeability for accumulation in tumor as well as long stokes shift [21,22]. As a typical kind of porphyrins, tetra(4-carboxyphenyl)porphine (TCPP) demonstrates itself as both an excellent PS agent and a good FL imaging probe, by not only generating ROS under irradiation efficiently, but also exhibiting strong fluorescence emission in the near-infrared region [23,24]. However, the poor water solubility and cell-membrane permeability greatly restrict the biomedical applications of TCPP, especially in FL imaging-guided PDT. Fortunately, it has been well-established that nanoparticles can transport organic molecules with poor water solubility and bad cell permeability into cells by neglecting their intrinsic properties [25–28]. Particularly, polymer nanoparticle is becoming an appealing platform for the preparation of multifunctional nanotheranostic probes because the rational design can be easily realized by judicious incorporation of building blocks [29–33]. For example, a simple amide coupling reaction was used to prepare TCPP-polyethylene glycol (PEG) based nanotheranostic probes for imaging-guided cancer therapy [34]. Although various reported nanotheranostic

* Corresponding author.
E-mail address: yichq@mail.sysu.edu.cn (C. Yi).
[1] These authors contributed equally to this work.

https://doi.org/10.1016/j.cclet.2022.01.049
1001-8417/

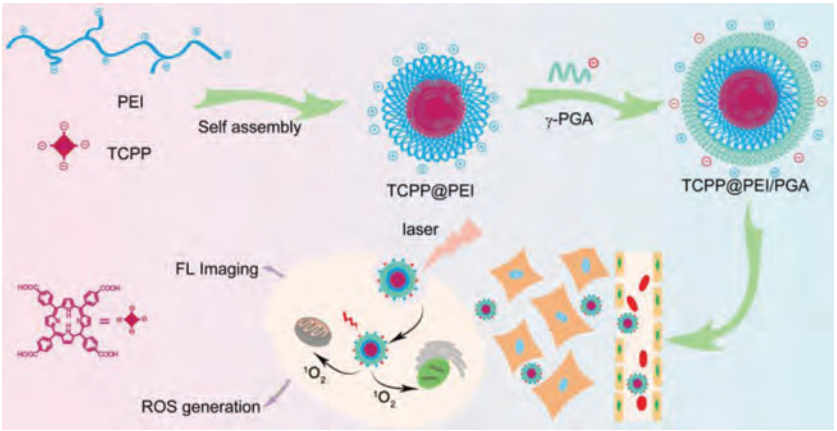

Scheme 1. Schematic illustration for the synthesis of TCPP@PEI/PGA nanoparticles and their applications in FL bioimaging *in vivo* and cell destruction *in vitro*.

probes exhibited excellent performance for cancer therapy, it is still compelling to develop simple but robust synthetic routes for the preparation of polymer nanotheranostics in a more efficient manner.

Polyethylenimine (PEI) presents itself as an attractive building block for the synthesis of polymer nanoprobes because of its features such as excellent water solubility and cell-membrane permeability aroused by its large amount of amino groups and positive charges [31-33,35-38]. More importantly, the electrostatic interaction between positively charged PEI and negatively charged TCPP can induce the self-assembly of PEI and TCPP to form polymer nanoparticles which can easily transport TCPP into cells by neglecting its intrinsic property. Therefore, a simple but robust synthetic route is successfully demonstrated to encapsulate TCPP into PEI-based nanotheranostic probes TCPP@PEI/PGA, and the potential of TCPP@PEI/PGA for FL imaging-guided PDT is initially evaluated using CT 26 cells and CT 26 tumor-bearing mice (Scheme 1).

Their large amount of amino groups make PEI positively charged and highly hydrophilic. More importantly, the amino groups of PEI can interact with carboxylic groups of TCPP to form nanoparticles *via* electrostatic interaction-induced self-assembly (Scheme 1), and thereafter improve the water solubility and cell-membrane permeability of TCPP. This can facilitate its biomedical applications, especially for FL imaging-guided PDT. From the perspectives of PDT and FL imaging, the as-prepared TCPP@PEI/PGA nanoparticles should have the strongest capability of $^1O_2$ genera-

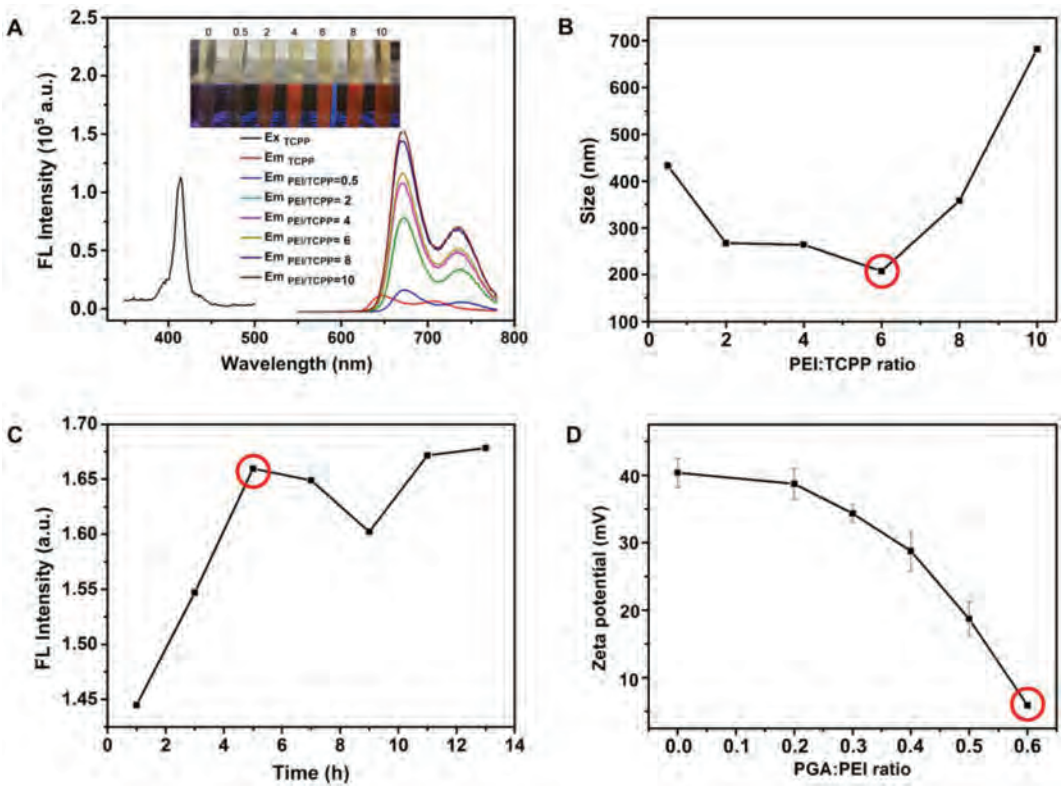

Fig. 1. Synthesis of TCPP@PEI/PGA nanoparticles. Optimization of PEI/TCPP ratios using FL intensity (A) and size (B) of as-prepared nanoparticles as the parameters. Insert: Photos of the suspensions containing as-prepared TCPP@PEI nanoparticles using different PEI/TCPP ratios in daylight (upper) and under UV irradiation (lower). (C) Optimization of synthesis time using FL intensity (λ_{em} = 672 nm) as the parameter. (D) Optimization of PGA/PEI ratios using zeta potential of as-prepared TCPP@PEI/PGA nanoparticles as the parameter.

tion as well as the highest FL quantum yield (QY). And from the perspective of *in vivo* application, nanoparticles with smaller diameter are advantageous. Therefore, the PEI/TCPP ratio and the reaction time for the nanoparticle synthesis were optimized at first. As shown in Fig. 1A and Fig. S1 (Supporting information), along with the increase of the PEI/TCPP ratio, the amount of undissolved TCPP decreased and the FL intensity of the nanoparticle suspension increased. And when the PEI/TCPP ratio reached 10, all the TCPP completely reacted with PEI to form nanoparticles (Inset of Fig. 1A). However, for the as-prepared TCPP@PEI/PGA nanoparticle, at the PEI/TCPP feed mass ratio of 6, its size minimized (Fig. 1B) as well as its FL QY and $^1O_2$ QY maximized (Table S1 in Supporting information). Considering that nanoparticles with smaller diameter, higher FL QY as well as $^1O_2$ QY are beneficial to *in vivo* biomedical applications, the PEI/TCPP ratio of 6 was considered as the optimal experiment condition for the synthesis. And from Fig. 1C, the FL intensity of the nanoparticle suspension was leveled off after reaction 5 h, *i.e.*, the optimal reaction time for the synthesis.

It has been well-documented that the excess of surface positive charge might also induce serious cytotoxicity. To address this issue, in this study, biocompatible γ-PGA was modified onto the surface of TCPP@PEI nanoparticles *via* electrostatic interaction between carboxylic groups of γ-PGA and amino groups of PEI. As expected, along with the increase of the PGA/PEI ratio from 0 to 0.6, the zeta potential of the as-prepared nanoparticles decreased from ~40.0 mV to ~6.0 mV (Fig. 1D). Since a certain amount of surface positive charge can facilitate the entry of nanoparticles into cells without affecting cell activity, the PGA/PEI ratio of 0.6 was considered as the optimal experiment condition for the surface modification.

As shown in TEM image, the as-prepared TCPP@PEI/PGA nanoparticles exhibited irregular sphericity (Fig. 2A). DLS measurements revealed that the water-dispersed TCPP@PEI/PGA nanoparticles exhibited an uniform size distribution with a hydrodynamic diameter of 221 ± 28.3 nm (Fig. 2B). And the surface modification with γ-PGA substantially decreased the zeta potential of TCPP@PEI/PGA nanoparticles to +5.91 mV.

The successful synthesis of TCPP@PEI/PGA nanoparticles was validated by the UV–vis absorption spectra and FL spectra. As demonstrated in Fig. 2C, TCPP exhibited the characteristic absorption peak at ~420 nm which was originated from the porphyrin moiety of TCPP, while all the other components for nanoparticle synthesis, PEI and PGA, barely had absorption at ~420 nm. However, both TCPP@PEI and TCPP@PEI/PGA nanoparticles exhibited the characteristic absorption of TCPP, indicating the successful encapsulation of TCPP into nanoparticles. Notably, TCPP@PEI/PGA nanoparticles also exhibited an absorption peak at ~660 nm (Inset of Fig. 2C), which could facilitate the PDT because the laser with longer wavelength is beneficial for *in vivo* applications.

Similarly, as demonstrated in Fig. 2D, TCPP exhibited the characteristic emission peaks at ~650 nm and ~710 nm upon excitation at 414 nm, while all the other components for nanoparticle synthesis, PEI and PGA, exhibited no emission behavior at the wavelength range of 600–780 nm. However, both TCPP@PEI and TCPP@PEI/PGA nanoparticles exhibited the characteristic emission peaks of TCPP, again indicating the successful encapsulation of TCPP into nanoparticles. Notably, compared with TCPP, a red shift of ~20 nm was observed in the wavelengths of emission peaks of TCPP@PEI nanoparticles and TCPP@PEI/PGA nanoparticles, possibly due to the abundant amino groups surrounding the TCPP [39,40]. The excellent emission property makes TCPP@PEI/PGA nanoparticle

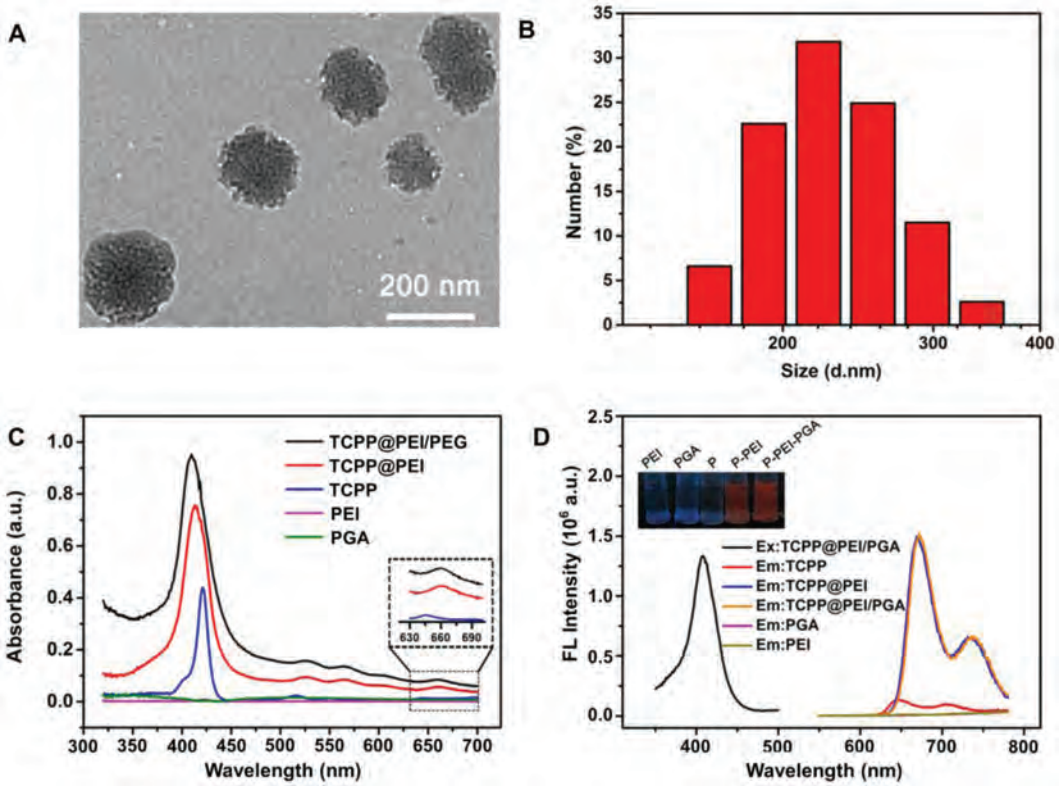

Fig. 2. Characterization of TCPP@PEI/PGA nanoparticles. (A) TEM image of TCPP@PEI/PGA nanoparticles. (B) Particle size distribution of TCPP@PEI/PGA nanoparticles. (C) The absorption spectra of TCPP, PEI, PGA, TCPP@PEI and TCPP@PEI/PGA nanoparticles. Insert: The enlarged absorption spectra of TCPP, TCPP@PEI and TCPP@PEI/PGA nanoparticles in the wavelength of 630–700 nm. (D) The fluorescence excitation spectrum of TCPP@PEI/PGA nanoparticles, and the emission spectra of TCPP, PEI, PGA, TCPP@PEI and TCPP@PEI/PGA nanoparticles. Insert: The photos of TCPP, PEI, PGA, TCPP@PEI and TCPP@PEI/PGA nanoparticles under UV irradiation.

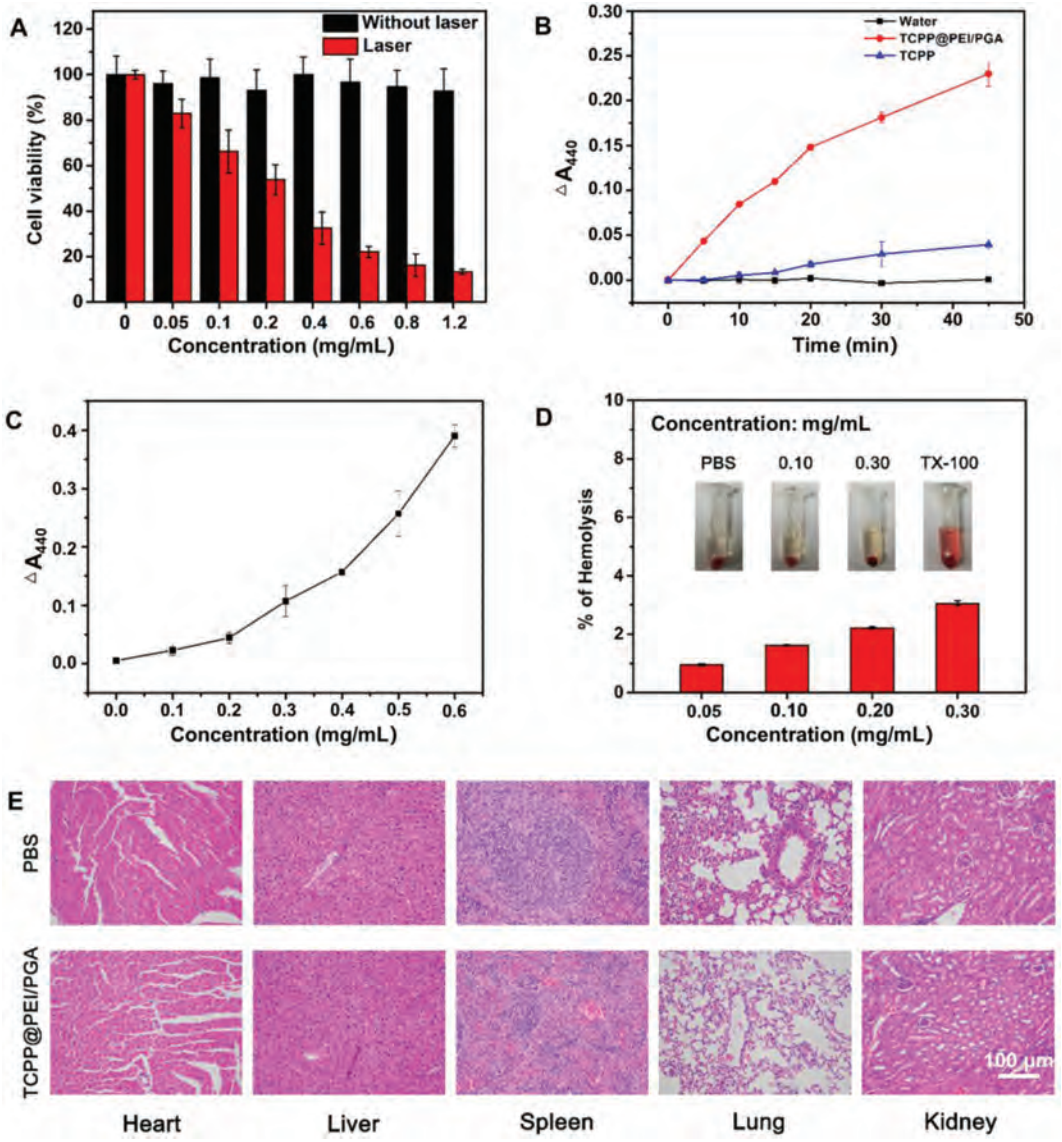

Fig. 3. Biotoxicity of TCPP@PEI/PGA nanoparticles. (A) Cell viabilities of CT26 cells upon treatment with TCPP@PEI/PGA nanoparticles with or without laser irradiation (650 nm, 0.1 W/cm^2, 10 min). (B) The time-dependent production of $^1O_2$ in the presence of 0.48 mg/mL of TCPP@PEI/PGA nanoparticles (red curve), TCPP (blue curve) and water (black curve) under 10 min laser irradiation. (C) The concentration-dependent production of $^1O_2$ in the presence of 0.48 mg/mL of TCPP@PEI/PGA nanoparticles under 10 min laser irradiation. (D) Hemolytic potential of TCPP@PEI/PGA nanoparticles to human red blood cells. (E) H&E staining of organs dissected from mice upon treatment with PBS and TCPP@PEI/PGA nanoparticles (0.80 mg/mL).

suitable for *in vivo* FL bioimaging applications. Since the synthesis reproducibility of TCPP@PEI/PGA nanoparticles is quite important for its future applications, we analyzed the key parameters, such as size, surface potential as well as emission properties, of 3 different batches of TCPP@PEI/PGA nanoparticles which were synthesized by 3 different graduate students. As shown in Table S2 (Supporting information), 3 different batches of as-prepared TCPP@PEI/PGA nanoparticles exhibited the similar size distribution profile, surface potentials and emission features. The quite simple and straightforward synthesis protocol definitely contributes to its good synthesis reproducibility.

The low cytotoxicity and good biocompatibility of TCPP@PEI/PGA nanoparticles were verified by the MTT assay, as evidenced by a high cell viability (~95%) even after being exposed to TCPP@PEI/PGA nanoparticles with a concentration as high as 1.20 mg/mL for 24 h (black bar of Fig. 3A). However, when the TCPP@PEI/PGA nanoparticle-treated CT26 cells were irradiated with a 650 nm laser (energy density: 0.1 W/cm^2) for 10 min, cell viability exhibited a concentration-dependent decrease (red bar of Fig. 3A). More than 90% of CT 26 cells were destructed at dosage of 1.20 mg/mL of TCPP@PEI/PGA nanoparticle and 10 min laser irradiation, indicating the high efficiency of cell destruction. It is believed that singlet oxygen ($^1O_2$) generated by TCPP@PEI/PGA nanoparticle upon laser irradiation should be responsible for the efficient cell destruction. Experiment results confirmed the time-dependent (red curve of Fig. 3B) and concentration-dependent (Fig. 3C) production of $^1O_2$ in the presence of 0.48 mg/mL of TCPP@PEI/PGA nanoparticles and 10 min laser irradiation, suggesting that TCPP@PEI/PGA nanoparticle is also a good PS candidate for tumor cell destruction through PDT. Correlated well with Table S1, the encapsulation of TCPP into TCPP@PEI/PGA did not obviously affect the capability of $^1O_2$ generation, as evidenced by that $^1O_2$ QY of TCPP and TCPP@PEI/PGA were 24.3% and 22.8%, respectively.

The good biocompatibility of TCPP@PEI/PGA nanoparticles was also verified by their low hemolytic efficiency when using hu-

man red blood cells as the model. As shown in Inset picture of Fig. 3D, TCPP@PEI/PGA nanoparticles with various concentrations did not cause the red blood cells to rupture and thereafter release hemoglobin, presenting no visually red color of the solution. Correlated well with this bare eye observation, only ~3.0% of hemolytic efficiency was determined for TCPP@PEI/PGA nanoparticles with the concentrations up to 0.30 mg/mL (Fig. 3D). All these results verified the excellent blood compatibility of TCPP@PEI/PGA nanoparticles.

The potential biotoxicity of TCPP@PEI/PGA nanoparticles was evaluated using Balb/c mice. After being intravenous injected with TCPP@PEI/PGA nanoparticles, the mice were dissected to collect main organs including heart, kidneys, lungs, liver, and spleen for H&E staining. As shown in Fig. 3E, compared to the PBS treated mice, all major organs of TCPP@PEI/PGA nanoparticle-treated mice exhibited negligible damage or inflammation. Again, this results further confirmed good biocompatibility and low biotoxicity of TCPP@PEI/PGA nanoparticles, laying a solid foundation for their *in vivo* bioimaging applications.

Encouraged by their good biocompatibility, the capabilities of TCPP@PEI/PGA nanoparticles for *in vitro* and *in vivo* FL bioimaging were demonstrated by the use of CT 26 cells, zebra fishes and Balb/c mice as models. The abundant surface amino groups of TCPP@PEI/PGA nanoparticles afforded themselves good cell-membrane permeability, because amino groups could arouse endosomolytic effect. Combined with their bright FL, TCPP@PEI/PGA nanoparticles are expected to be effective FL imaging probes. The good cell-membrane permeability of TCPP@PEI-PGA nanoparticles were validated by the red cellular fluorescence (Fig. 4A). To reveal the location of TCPP@PEI/PGA nanoparticles in the cells after endocytosis, TCPP@PEI/PGA nanoparticle-treated cells were further treated with DAPI which could specifically stain the cell nuclei. Fig. 4A clearly showed that TCPP@PEI/PGA nanoparticles were mainly localized in the cytoplasmic region of the cells, suggesting the efficient internalization and accumulation of TCPP@PEI/PGA nanoparticles in tumor cells. In addition, the intact morphology of TCPP@PEI/PGA nanoparticle-treated cells also confirmed the good biocompatibility of TCPP@PEI/PGA nanoparticles.

The capabilities of TCPP@PEI/PGA nanoparticles for *in vivo* FL bioimaging were firstly evaluated using zebra fishes. Fig. 4B clearly showed that zebra fishes can uptake TCPP@PEI/PGA nanoparticles without affecting their normal physiological behaviors, as evidenced by the obvious and bright red fluorescence at their esophagus. This result suggested that zebra fishes might uptake TCPP@PEI/PGA nanoparticles *via* swallowing behavior. Again, the good biocompatibility and the low biotoxicity of TCPP@PEI/PGA nanoparticles was also verified by that TCPP@PEI/PGA nanoparticle-treated zebra fishes exhibited the intact morphology without obvious lesion and/or teratogenesis.

Balb/c mice were also used as model to evaluate the bioimaging capability of TCPP@PEI/PGA nanoparticles. All animal experiments were performed in compliance with the regulations of the Animal Ethical and Welfare Committee of Sun Yat-sen University. Fig. 4C showed real-time *in vivo* imaging of mice at different time points after being intravenous injected with TCPP@PEI/PGA nanoparticles. 1 h after tail vein injection, strong FL signals originated from TCPP@PEI/PGA nanoparticles could be clearly observed in kidney, and the intensity of FL signals in kidney decreased along with time (middle of Fig. 4C). This result suggested that TCPP@PEI/PGA nanoparticles could be efficiently accumulated in kidney and renal excretion was the main elimination route for TCPP@PEI/PGA nanoparticles. In addition, 24 h after tail vein injection, the efficient accumulation of TCPP@PEI/PGA nanoparticles in liver was also confirmed (upper of Fig. 4C), suggesting that nanoparticles could also be eliminated by enteron excretion. Through imaging of the single organ after dissection, the accumulation of TCPP@PEI/PGA nanoparticles in lung was also observed (lower of Fig. 4C), possibly due to the reticuloendothelial system containing large amounts of phagocytosis in lung [41]. It was also worthy to mention that FL signals were barely observed from the heart, and spleen. All imaging results revealed that the synergistic metabolism of TCPP@PEI/PGA nanoparticles *via* kidney and liver.

Encouraged by the excellent PDT efficiency of TCPP@PEI/PGA nanoparticles *in vitro*, a preliminary anti-tumor study using CT 26 tumor-bearing mice was carried out to assess its feasibility as PDT agent for cancer therapy *in vivo*. As shown in Fig. S2 (Supporting information), tumor volume was significantly decreased after being treated with 100 μL TCPP@PEI/PGA (0.80 mg/mL) and laser irradiation under a 635 nm laser (25 mW/cm^2) for 10 min. The results indicated that TCPP@PEI/PGA nanoparticles exhibited potential in tumor growth inhibition and FL imaging-guided phototherapy.

In conclusion, a simple and robust synthetic route is successfully demonstrated to encapsulate the porphyrin derivative, TCPP,

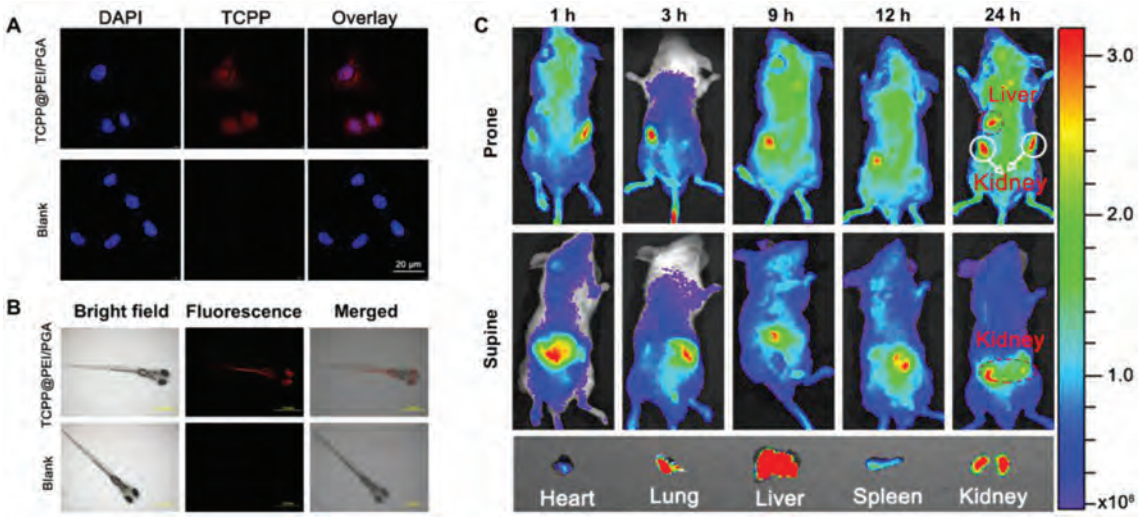

Fig. 4. Bioimaging applications of TCPP@PEI/PGA nanoparticles. (A) CLSM images of CT 26 cells incubated with and without TCPP@PEI/PGA nanoparticles. The nuclei were stained with DAPI (blue). (B) Bright-field and fluorescence images of zebra fishes upon treatment with and without TCPP@PEI/PGA nanoparticles. (C) *In vivo* FL imaging of mice after intravenous injection with TCPP@PEI/PGA nanoparticles at different time points, and *ex vivo* FL images examined at 24 h post-injection.

into PEI-based polymer nanotheranostics, TCPP@PEI/PGA nanoparticles, for *in vivo* bioimaging applications. In the resultant nanotheranostics, TCPP serves a dual function as the FL imaging probe and the PS for PDT. *In vitro* and *in vivo* experiments confirmed that TCPP@PEI/PGA nanoparticles exhibited excellent biocompatibility as well as efficient FL imaging capability. In addition, *in vitro* and *in vivo* experiments validated that TCPP@PEI/PGA nanoparticles could also serve as an effective phototherapeutic agent for cancer cell killing and tumor growth inhibition by generating efficient $^1O_2$ under a 650 nm laser irradiation. All the results validated that TCPP@PEI/PGA nanoparticles were high efficient theranostic probes for *in vivo* applications.

Declaration of competing interest

The authors declare that they have no known competing financial interests or personal relationships that could have appeared to influence the work reported in this paper.

Acknowledgments

The financial support from Shenzhen Basic Research Program (No. JCYJ20210324140004013), Guangdong Provincial Key Laboratory of Sensing Technology and Biomedical Instruments (No. 2020B1212060077), and Guangdong Natural Science Foundation (No. 2020A1515010661) is gratefully acknowledged.

Supplementary materials

Supplementary material associated with this article can be found, in the online version, at doi:10.1016/j.cclet.2022.01.049.

References

[1] M.J. Manyak, A. Russo, P.D. Smith, et al., J. Clin. Oncol. 6 (1988) 380–391.
[2] M. Wainwright, Chem. Soc. Rev. 25 (1996) 351–359.
[3] K. Yan, Y. Zhang, C. Mu, et al., Theranostics 10 (2020) 7287–7318.
[4] J.M. Chen, T.J. Fan, Z.J. Xie, et al., Biomaterials 23 (2020) 119827.
[5] J.C. Li, K.Y. Pu, Acc. Chem. Res. 53 (2020) 752–762.
[6] X.M. Cheng, J. Gao, Y. Ding, et al., Adv. Sci. (2021) 2100876.
[7] T.T. Hu, Z.D. Wang, W.C. Shen, et al., Theranostics 11 (2021) 3278–3300.
[8] H.Y. Yang, R.F. Liu, Y.X. Xu, et al., Nano-Micro Lett. 13 (2021) 35.
[9] J.C.S. Simoes, S. Sarpaki, P. Papadimitroulas, et al., J. Med. Chem. 63 (2020) 14119–14150.
[10] H.F. Wen, Z.J. Zhang, M.M. Kang, et al., Biomaterials 274 (2021) 120892.
[11] Y.P. Jiang, W. Meng, L.J. Wu, et al., Adv. Healthc. Mater. 10 (2021) 2100789.
[12] G. Yuan, C. Lv, J.C. Liang, et al., Adv. Funct. Mater. 31 (2021) 2104026.
[13] L. Li, Y.S. Chen, W.J. Chen, et al., Chin. Chem. Lett. 30 (2019) 1689–1703.
[14] J. Tian, B.X. Huang, M.H. Nawaz, et al., Coord. Chem. Rev. 420 (2020) 213410.
[15] B.R. Xie, Y. Yu, X.H. Liu, et al., Biomaterials 272 (2021) 120782.
[16] B. Wang, Y.N.Dai B, Y.J. Kong, et al., ACS Appl. Mater. Interfaces 12 (2020) 53634–53645.
[17] S.J. Qi, N. Kwon, Y. Yim, et al., Chem. Sci. 11 (2020) 6479–6484.
[18] Y. Zhu, W.H. Lin, W. Zhang, et al., Chin. Chem. Lett. 28 (2017) 1875–1877.
[19] K. Deng, Z. Hou, X. Deng, et al., Adv. Funct. Mater. 25 (2015) 7280–7290.
[20] Z. Sheng, D. Hu, M. Xue, et al., Nano-Micro Lett. 5 (2013) 145–150.
[21] Y.M. Zhou, X.L. Liang, Z.F. Dai, Nanoscale 8 (2016) 12394–12405.
[22] J.M. Park, K.I. Hong, H. Lee, et al., Accounts Chem. Res. 54 (2021) 2249–2260.
[23] J.J. Liu, Y. Yang, W.W. Zhu, et al., Biomaterials 97 (2016) 1–9.
[24] L.F. Hang, T. Zhang, H. Wen, et al., Nano Res. 14 (2020) 660–666.
[25] Z. Zhang, Y. Shi, Y. Pan, et al., J. Mat. Chem. B. 2 (2014) 5020–5027.
[26] Y. Shi, H. Zhang, Z. Yue, et al., Nanotechnology 24 (2013) 375501.
[27] P. Pal, S.K. Rastogi, C.M. Gibson, et al., ACS Appl. Mater. Interfaces 3 (2011) 279–286.
[28] S.K. Rastogi, P. Pal, D.E. Aston, et al., ACS Appl. Mater. Interfaces 3 (2011) 1731–1739.
[29] L. Feng, C. Zhu, H. Yuan, et al., Chem. Soc. Rev. 42 (2013) 6620–6633.
[30] J. Ramos, J. Forcada, R. Hidalgo-Alvarez, Chem. Rev. 114 (2014) 367–428.
[31] W. Chen, Q. Wang, J. Ma, et al., Mikrochim. Acta 185 (2018) 523.
[32] Q. Wang, Y. Shi, W. Chen, et al., Mikrochim. Acta 188 (2021) 9.
[33] Y. Shi, Z. Chen, X. Cheng, et al., Biosens. Bioelectron 61 (2014) 397–403.
[34] L. Cheng, D.W. Jiang, A. Kamkaew, Adv. Funct. Mater. 27 (2017) 1702928.
[35] Y. Pan, W.D. Chen, J. Yang, et al., Anal. Chem. 90 (2018) 1992–2000.
[36] Y.N. Fang, J. Jia, Jun Yang, et al., Chin. Chem. Lett. 29 (2018) 1277–1280.
[37] Y.P. Shi, Y. Pan, J. Zhong, et al., Carbon 93 (2015) 742–750.
[38] Y. Pan, J. Yang, Y.N. Fang, et al., J. Mat. Chem. B 5 (2017) 92–101.
[39] Z.M. Zhang, Y. Pan, Y.N. Fang, et al., Nanoscale 8 (2016) 500–507.
[40] Y.N. Fang, L.F. Zhou, J. Yang, et al., ACS Appl. Bio Mater. 3 (2020) 3761–3769.
[41] L. Grislain, P. Couvreur, V. Lenaerts, et al., Int. J. Pharm. 15 (1983) 335–345.